[20] C. Valenta and G. Durgin, "Rectenna performance under power-optimized waveform excitation," in *Proc. 2013 IEEE Int. Conf. RFID*, pp. 237–244.
[21] C. Maldonado-Codina and N. Efron, "Impact of manufacturing technology and material composition on the surface characteristics of hydrogel contact lenses," *Clinical Experimental Optometry: J. Australian Optometrical Assoc.*, vol. 88, pp. 396–404, Nov. 2005.
[22] A. Peyman, S. Holden, and C. Gabriel, "Dielectric properties of tissues at microwave frequencies," Mobile Telecommunications and Health Research Programme, Chilton, Didcot, Oxfordshire, U.K. [Online]. Available: https://www.researchgate.net/profile/Simon_Holden/publication/242720097_Mobile_Telecommunications_and_Health_Research_Programme_Dielectric_Properties_of_Tissues_at_Microwave_Frequencies/links/555d953108ae9963a1127ae3/Mobile-Telecommunications-and-Health-Research-Programme-Dielectric-Properties-of-Tissues-at-Microwave-Frequencies.pdf
[23] C. Gabriel. (2015). Dielectric properties of body tissues. [Online]. Available: http://niremf.ifac.cnr.it/tissprop/htmlclie/htmlclie.php
[24] T. Wessapan and P. Rattanadecho, "Specific absorption rate and temperature increase in human eye subjected to electromagnetic fields at 900 MHz," *Trans. ASME, J. Heat Transf.*, vol. 134, no. 9, pp. 1–11, 2012.
[25] A. Shameli, A. Safarian, A. Rofougaran, M. Rofougaran, and F. De Flaviis, "Power harvester design for passive UHF RFID tag using a voltage boosting technique," *IEEE Trans. Microw. Theory Techn.*, vol. 55, no. 6, pp. 1089–1097, 2007.
[26] M. Roberg, T. Reveyrand, I. Ramos, E. A. Falkenstein, and Z. Popovi, "High-efficiency harmonically terminated diode and transistor rectifiers," *IEEE Trans. Microw. Theory Techn.*, vol. 60, no. 12, pp. 4043–4052, 2012.
[27] K. Hosain, A. Z. Kouzani, S. Tye, A. Kaynak, and M. Berk, "RF rectifiers for EM power harvesting in a deep brain stimulating device," *Australasian Physical Eng. Sci. Med.*, vol. 38, pp. 157–172, Mar. 2015.
[28] Y. T. Liao, H. Yao, A. Lingley, B. Parviz, and B. P. Otis, "A 3 μw CMOS glucose sensor for wireless contact-lens tear glucose monitoring," *IEEE J. Solid-State Circuits*, vol. 47, pp. 335–344, Jan. 2012.
[29] E. Y. Chow, A. L. Chlebowski, and P. P. Irazoqui, "A miniature-implantable RF-wireless active glaucoma intraocular pressure monitor," *IEEE Trans. Biomed. Circuits Syst.*, vol. 4, pp. 340–349, Dec. 2010.
[30] K. Raizada and M. Sridhar, "Nomogram for spherical RGP contact lens fitting in patients with pellucid marginal corneal degeneration (PMCD)," *Eye Contact Lens*, vol. 29, no. 3, pp. 168–172, 2003.

Wireless Sensor Network Utilizing Radio-Frequency Energy Harvesting for Smart Building Applications

O. Björkqvist, O. Dahlberg, G. Silver, C.I. Kolitsidas, O. Quevedo-Teruel, and B.L.G. Jonsson

The scope of this article is to develop a modular radio-frequency (RF) energy-harvesting system for smart buildings that can act as a power source for sensing devices. Electromagnetic field-strength measurements at the main campus of the KTH Royal Institute of Technology in Stockholm, Sweden, were carried out to define the strength of the available ambient signals. Mainly two spectra were available for possible RF harvesting, i.e., two cellular bands [GSM1800 and third generation (3G)] and the 2.45-GHz Wi-Fi band. Based on these measurements, a modular approach for the system was adopted. The system is composed from two modules: 1) a Wi-Fi rectenna system composed of eight dual-polarized patch antennas and 16 rectifiers to produce eight differential voltage sources connected in series and 2) a cellular rectenna system composed of eight linear tapered slot antennas and eight rectifiers to produce four differential voltage sources connected in series. We propose an innovative multiple-input, single-output (MISO) wave rectifier that yields an efficient differential output. Both rectenna modules offer full azimuthal coverage and can operate either together or independently.

EDITOR'S NOTE

Karl F. Warnick

This second article in this issue's "Education Corner" column was developed as part of the 2016 IEEE Antennas and Propagation Student Design Contest and received first prize. The system was designed and constructed according to the rules stated for the competition, i.e., the size shall not exceed $50 \times 50 \times 50$ cm^3. Also, during the design, construction, and measurement process, the primary goal was to make it educational and exciting for the participating students. All of the work was carried by the three third-year students with the help of three supervisors. The competition proved to be an excellent motivation for the students to be introduced into the antenna world and helped them develop a strong interest for the subject. All of the construction and measurements were performed at the facilities of the Antenna Laboratory at the Department of Electromagnetic Engineering at the KTH Royal Institute of Technology, Stockholm, Sweden.

Digital Object Identifier 10.1109/MAP.2018.2859196
Date of publication: 4 October 2018

INTRODUCTION TO ENERGY HARVESTING

Without a doubt, the Internet has created a revolution in how we interact, learn, and acquire information. Currently, we have almost 25 billion connected devices, which is approximately 3.5 times the population of Earth. We are on the edge of a new evolution where everything will be connected. This will bridge the physical world with the computer world, resulting in new ways of interaction. This interaction and integration of the two worlds will result in efficient and accurate control of the physical world. Essential improvement factors are minimal environmental impact, energy consumption, and cost. The next-generation communication networks will also focus on machine/environment-to-man, machine/environment-to-machine, and machine/environment-to-infrastructure communications. Sensors are going to be in the center of this evolution because they provide measures of the current state of the physical world with the ability to keep historical measurement data. Data from sensors are interfaced with the computer world, and, in turn, computers can provide critical information on the state of the system. Thus, developing autonomous and energy-efficient sensors is vital. For an autonomous system, one important factor is the power supply. A very appealing solution is to use the ambient RF energy that exists in a modern city environment from all of the wireless services, such as cell phones, Wi-Fi, and digital TV. Harvesting the ambient RF energy in a city environment has advantages because it does not depend on such uncontrollable external factors as solar energy or wind power.

A key application of future networks is expected to be smart buildings and smart cities. To be able to characterize a system as *smart*, it should be able to measure its own current state in the sense of self-awareness and provide feedback to the infrastructure. The scope of this article is to develop an RF energy-harvesting interface that will be able to power sensing devices for smart building applications. In our study, we use the main campus of KTH Royal Institute of Technology as our test environment for the system under development.

To date, a multitude of different harvesters have been presented for many different applications and scenarios. In 2014, a rigorous survey of the presented results in harvesting was conducted by Valenta and Durgin in [1]. In this article, the basic theory of RF energy harvesting was reviewed, and a comparative study with current state-of-the-art literature was performed in terms of harvesting efficiency with respect to input power. It is evident that the input RF power significantly affects the harvesting efficiency. There are several different harvester designs presented in the literature. Most designs can be categorized in one of the two approaches, rectennas utilizing either omnidirectional or directional antennas. This separation of approaches makes coverage with lower power feasible for RF ambient harvesting.

To obtain a highly efficient harvester, high-gain antennas are usually needed. In [2], a quad-band RF energy harvester is presented that was designed with the use of a genetic algorithm and operates in the 900-, 1,750-, 2,150-, and 2,450-MHz bands. The harvester employees a single dual-polarized patch antenna, which makes the harvester efficient for harvesting two polarizations but missing the third. Similarly, in [3], a differentially fed patch antenna is presented. As in [2], a directive antenna is used for increased rectifier efficiency at the expense of coverage. Moreover, the concept of differential field sampling and differential rectification is introduced. In [4] and [5], a novel concept was introduced for increasing power available at the rectifier by placing multiple antennas in an antenna array configuration.

An alternative approach to obtain a wider coverage is to use omnidirectional antennas. In [6], a wide-band bent triangular monopole antenna is presented. This approach enables harvesting for one polarization in the full azimuthal space. A similar work was presented in [7], where a miniaturized dual-band omnidirectional rectenna is proposed. The largest dimension of the antenna is $\lambda/3$ in the low frequency. This poses difficulties when wide bandwidth is desired. In [8], the authors match the antenna to the rectifying circuit, resulting in a wider operation band. Although giving the desired coverage, at least for one polarization, the approach utilizing omnidirectional antennas results in less received power and a lower efficiency of the harvester. Moreover, in these works, the antenna only captures one polarization, which in a multiscattering environment results in a loss of power in the other polarization. In our work, we combine the two solutions, employing multiple high-gain antennas, spatially displaced to ensure full coverage to enable ambient harvesting at low power levels. The power from each antenna element is rectified individually and then combined into a single output.

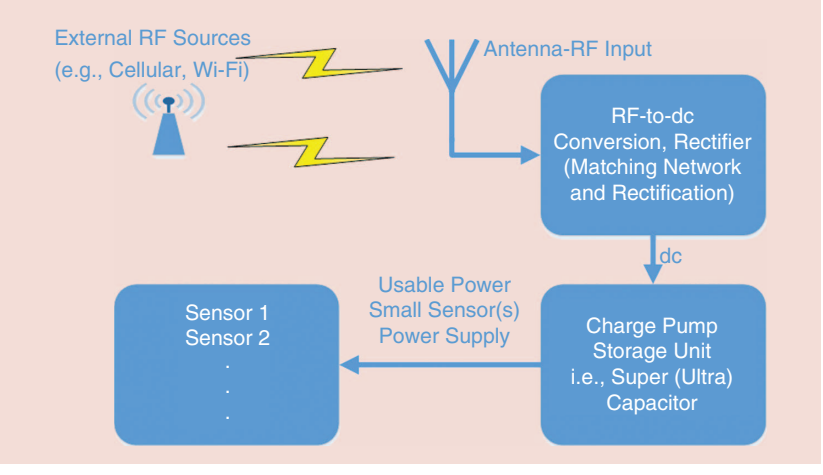

FIGURE 1. A general block diagram of an RF harvesting circuit.

The harvester needs to be designed for the operation environment, taking into account such factors as available spectrum, input power levels, and polarization of fields. Based on our initial field-strength measurements, a modular approach was adopted to use adaptivity for the available spectra. The typical components of an RF power scavenger are [9] the antenna that acts as the interface for the external RF signal, the rectifier that consists of an RF-to-dc conversion, a charge pump if required, and the energy storage unit and/or the load, which can be any sensing device, as depicted in Figure 1. The combination of an antenna and a rectifier is commonly known as a *rectenna* [10] and could be used in many different low-power applications where it is of interest to remove the need of batteries and cables to an external power supply.

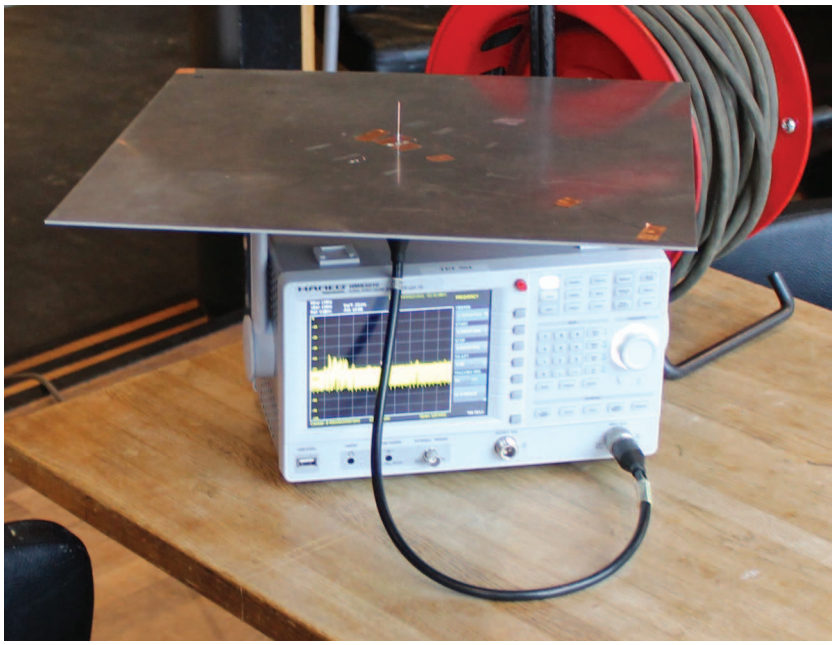

FIGURE 2. The measurement setup with the spectrum analyzer and one of the monopoles.

In this article, we introduce a novel configuration of directive antennas in a cuboid approach using both broadside and endfire radiation patterns for full azimuthal coverage. The outputs of the antennas are combined at per face per polarization per operational frequency to produce a differentially rectified output. This work was entered in the 2016 IEEE Antennas and Propagation Society (AP-S) Student Design Contest held at the IEEE AP-S Antennas and Propagation Symposium in Puerto Rico (see the "Editor's Note" box on page 124).

ELECTROMAGNETIC FIELD-STRENGTH MEASUREMENTS

Assessing the ambient levels of RF signals in the intended working

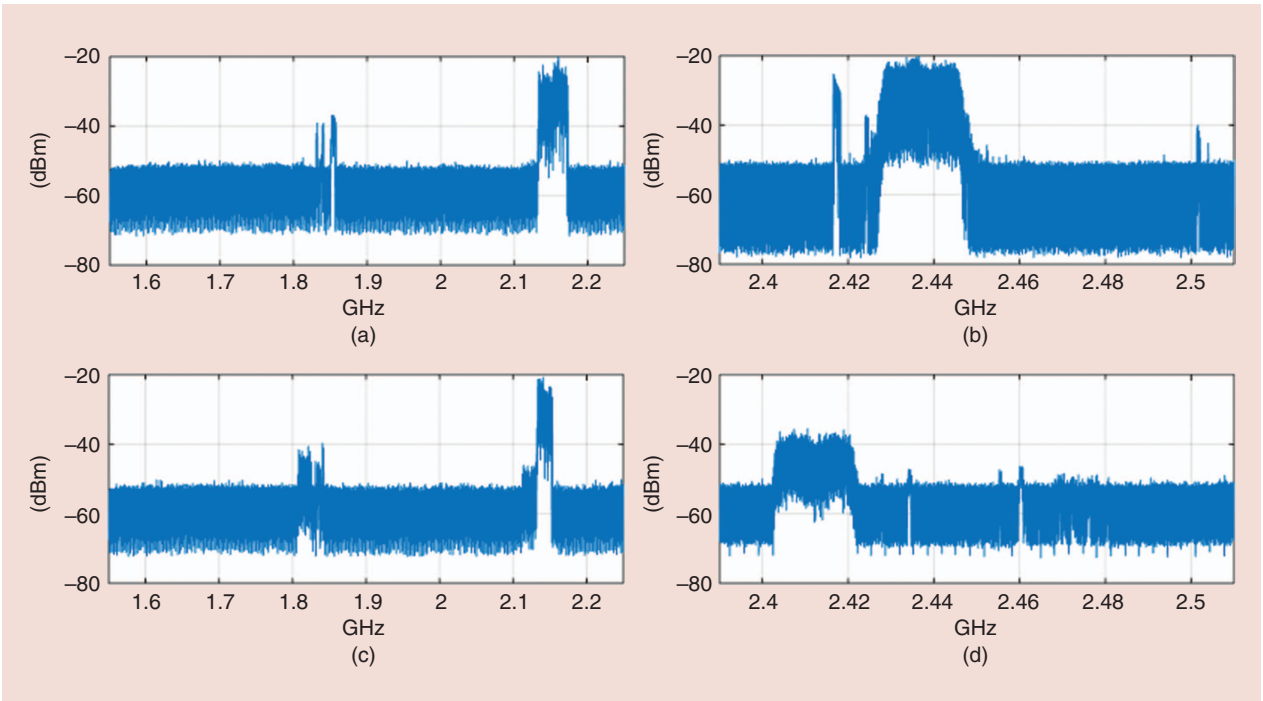

FIGURE 3. The measurements of ambient signals with power levels that can be harvested within the KTH campus using the monopole antennas. (a) Inside the building, (b) close to the Wi-Fi router, and (c) and (d) outside the building.

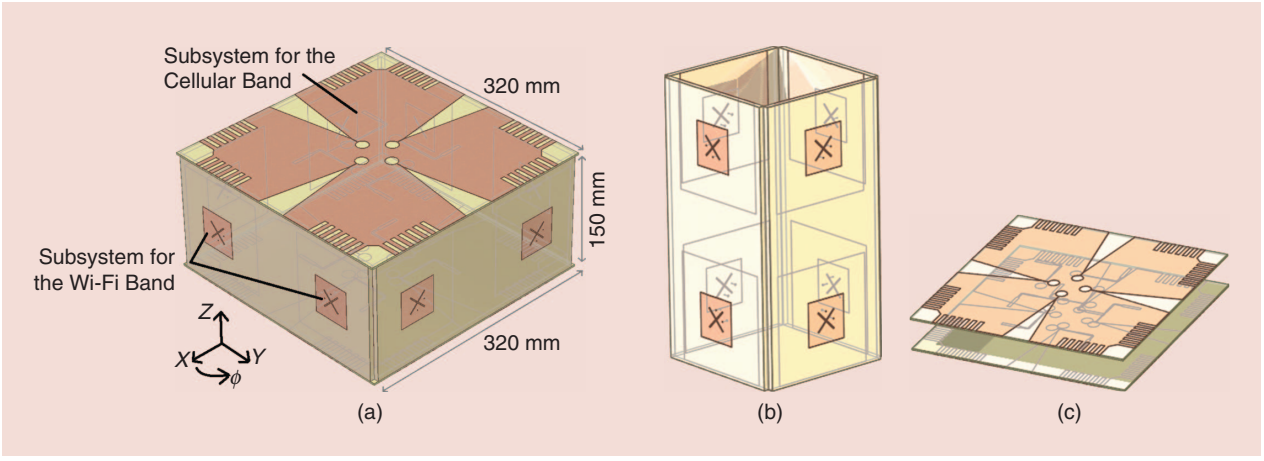

FIGURE 4. Schematics of (a) the full system, (b) the system if only Wi-Fi is harvested, and (c) the system if only cellular bands are harvested. (The constructed prototype is presented in Figure 17.)

environment of the harvester is the first important step in the design procedure of an RF harvesting system. A survey performed by Piñuela et al. [11] showed that, in an urban environment, the interesting RF bands are 3G, GSM, and Wi-Fi. Aiming for smart building applications at the KTH main campus, the available frequency bands and their power levels, in our environment, need to be determined. This is important because countries allocate different cellular bands for communications, although Wi-Fi remains the same. Usable ambient signals for RF harvesting are considered to be signals with power levels ≥ -40 dBm. The choice of this limit is based on the fact that the RF-to-dc conversion efficiency of a Schottky diode below this level is very low, and the output from the rectifier is virtually zero. To determine the available frequencies on the KTH campus, we measured in the first step with a wide-band log-periodic antenna connected to a spectrum analyzer, a HAMEG HMS3910. To perform such measurements, we enabled the peak detector with the hold peak option for approximately 10 min. In this way, we could determine useful levels of RF signal. This initial measurement resulted in three bands that provide good enough levels for RF harvesting: two cellular 1.8 and 2.1 GHz and the low band of the Wi-Fi 2.4 GHz. As a follow-up measurement, we constructed monopole antennas for the 1.8-, 2.1-, and 2.4-GHz bands. The monopole antenna

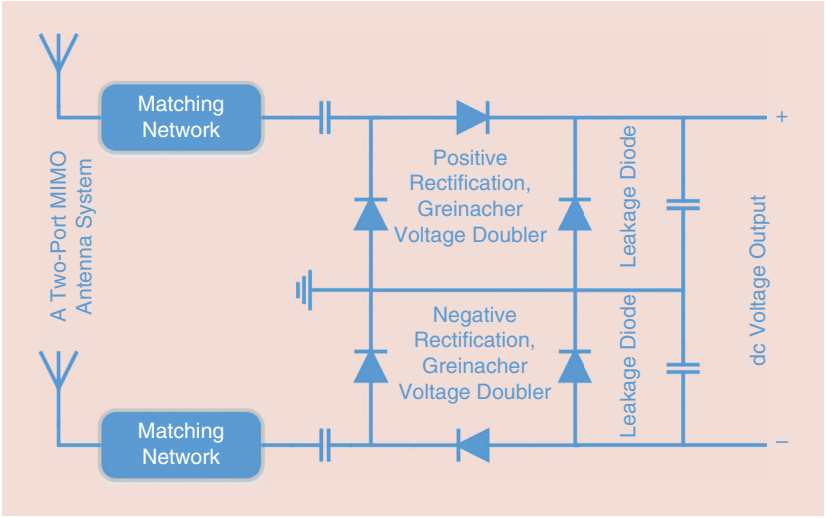

FIGURE 5. The differential MISO rectification. MIMO: multiple-input, multiple-output.

has a rotational symmetric radiation pattern that is ideal to determine levels of one single vertical polarization, covering the full azimuthal plane.

With the monopoles, one of which is illustrated in Figure 2, a second measurement campaign was performed in various places on the KTH campus, considering five different scenarios: indoors, semi-indoors, outdoors, semi-outdoors, and basements/underground laboratories. As semi-indoors, we consider the large open-space places that are located inside buildings and have at least one glass wall, i.e., a foyer; whereas for semioutdoors, we consider open spaces in close proximity of a building, such as a terrace. The measurements reveal that the cellular and the Wi-Fi signals are of different levels in these scenarios, and, in some cases, one of the two can be completely absent, i.e., in the basement no cellular signal was detected. Some representative measurements using the monopole antennas inside and outside our building at KTH are depicted in Figure 3. This measurement campaign motivates the idea to develop a modular system. What can be observed from the follow-up measurements is that the received power is at best –20 dBm when using omnidirectional monopole antennas. This further motivates our approach to employ directive antennas in a cube configuration to cover the entire azimuthal space. In the following analysis, we have assumed

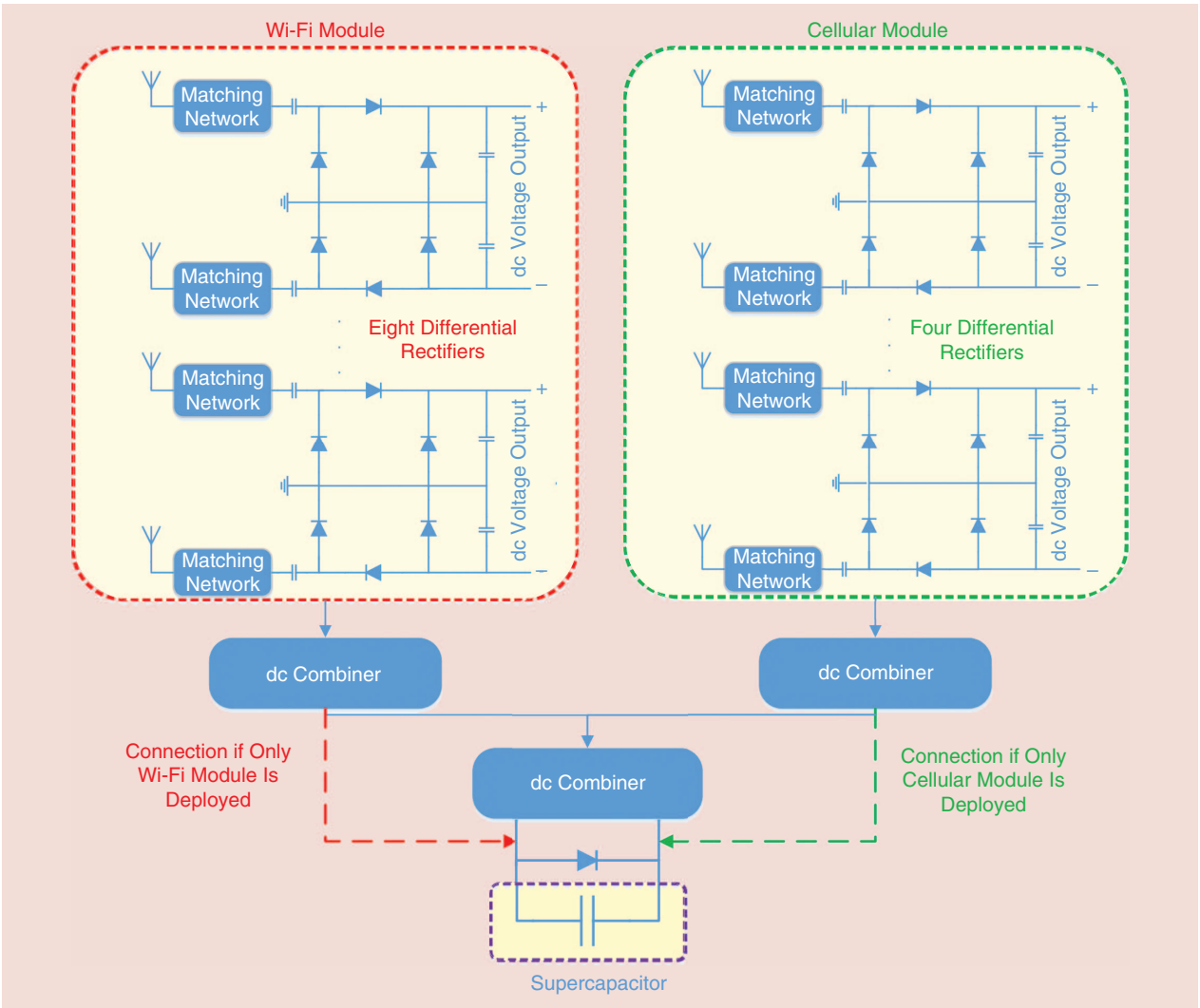

FIGURE 6. The power combiner and modularity of the system.

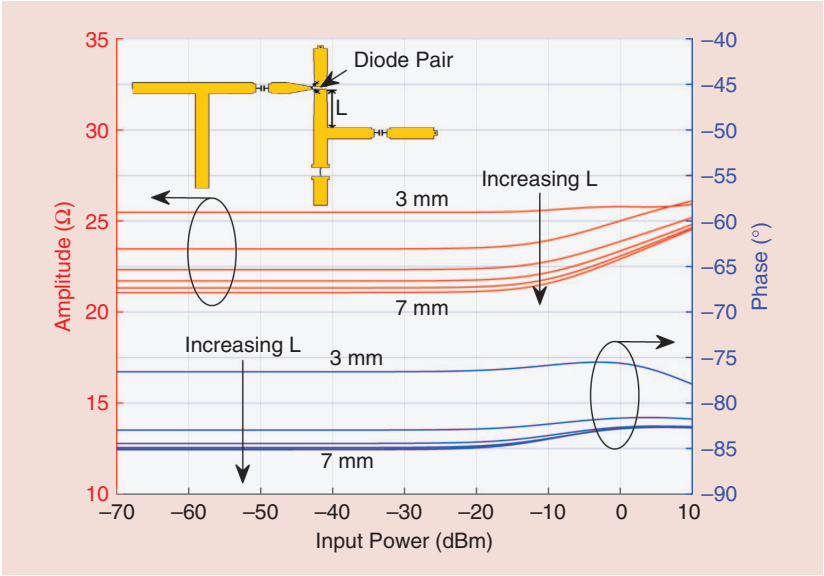

FIGURE 7. How the input impedance of the dc part varies with changing of the length L (from 3 to 7 mm with a step size of 0.8 mm); see the inset for the corresponding line dimension at the dc part.

–15 dBm as input power level calibrating for a directional antenna.

SYSTEM DESCRIPTION

The RF energy-harvesting system is designed to be operable in the 1.7–2.2- and 2.4–2.5-GHz bands. From the scenarios in the "Electromagnetic Field-Strength Measurements" section, it was observed that there are cases where either the cellular or the Wi-Fi system is redundant, and thus modularity can help design the systems in such a way that they can work either jointly or as standalone devices. RF harvesting systems often use omnidirectional antennas [6], [11], [12], but this results in a low gain, and the system then relies only on high levels of available RF power. In our developed system, directional antennas are employed.

They are placed on the device such that full azimuthal coverage is obtained. We adopted a rectangular parallele-piped-cuboid approach with antennas on all six faces. We use four out of six faces for the Wi-Fi band and the remaining two for the cellular band. An overview of the system and the modularity of the two subsystems is illustrated in Figure 4. Patch antennas are used for the Wi-Fi band, and linear tapered slot antennas (LTSAs) are used for the cellular bands. The choice of the LTSA serves a dual purpose. Primarily, it is an endfire radiating antenna [13], and thus the radiation pattern can cover the azimuthal space by placing four antennas, one in each 90° sector, covering two faces with eight antennas. The second reason for choosing the LTSA is because of its wide-band properties [14] that can cover all of the allocated bands for the 3G signal around the world.

We have also extended the full-wave rectification to a MISO perspective. By employing two antennas receiving in the same polarization and using a Greinacher voltage doubler [15] in each antenna, we use positive and negative rectification, resulting in a differential output voltage. This concept and the MISO full-wave retification are depicted in Figure 5.

One advantage of this configuration is that, by using a two-input MISO antenna system, we decrease the lowest level feasible for harvesting, as compared to a full-wave rectifier that uses a power divider and four Schottky diodes for the same input signal. Moreover, if all RF signals are combined at the RF domain, instead of the dc power, a radiation pattern is enforced, and an inherent circular array mode is excited. This approach, on the other hand, adds complexity and increases the size of the system. In addition, as depicted in Figure 5, one more diode is used, per antenna, to short-circuit the capacitor on the dc output side in the case of a reverse current. This current can appear if the levels of the incident signal vary between the two antennas. In this case, the two dc capacitors will charge in different levels, creating a voltage difference resulting in a discharge current. This scenario can occur, e.g., when this system is placed in close proximity to a Wi-Fi router. The diode avoids this effect with a minimal efficiency drop.

We evaluate the performance of the system by its efficiency. The efficiency of the rectenna system [16] can be defined as

$$\eta = \frac{P_{\mathrm{dc}}}{P_{\mathrm{RF}}}, \tag{1}$$

where P_{dc} is the dc output power, and P_{RF} is the output power delivered from the antenna port. Note that the antenna efficiency is not taken into account. This is because the antennas in our system have high efficiency [17], [18], around 90%, whereas the rectifier efficiency is considerably less. The dc power is given by

$$P_{\mathrm{dc}} = \frac{V_{\mathrm{dc}}^2}{R_{\mathrm{Load}}}, \tag{2}$$

where V_{dc} is the voltage over the load and R_{Load} is the load resistance. The use of two antennas results in a doubling of the available RF power at the rectifier. This results in an approximate doubling of the output voltage, with the same levels of ambient fields, resulting in a doubling of the rectifier efficiency according to

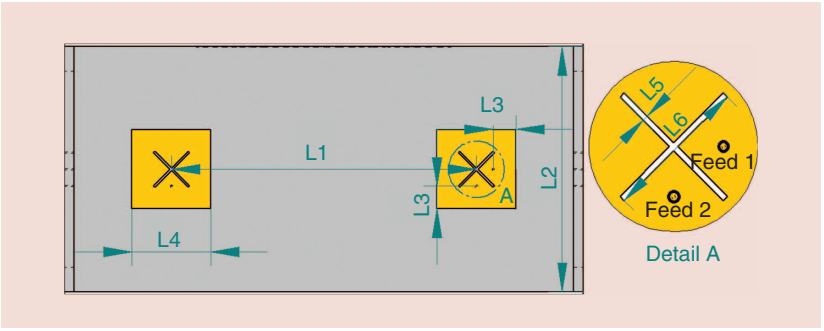

FIGURE 8. A side view of the Wi-Fi module, two patch antennas.

TABLE 1. THE DIMENSIONS FOR THE PATCH ANTENNA.

Parameter	Value	Parameter	Value
L1	200 mm	L4	48.6 mm
L2	150 mm	L5	1.2 mm
L3	14 mm	L6	30 mm

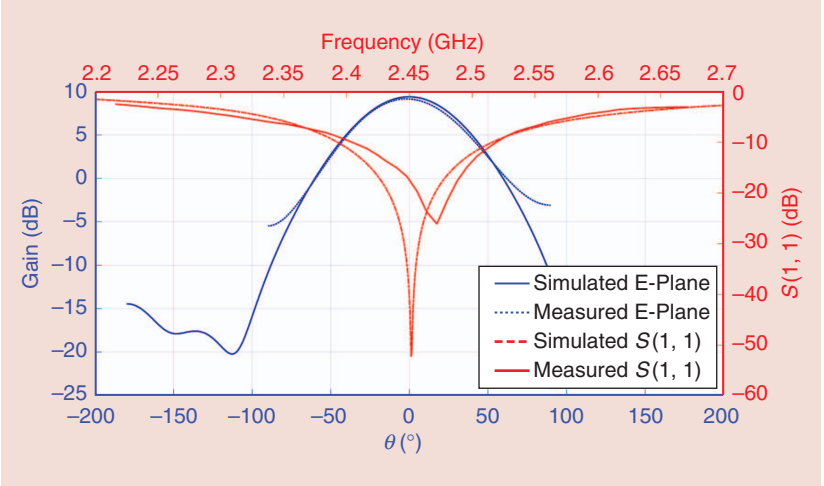

FIGURE 9. The far-field (E-plane at 2.45 GHz) and reflection coefficients from a single patch.

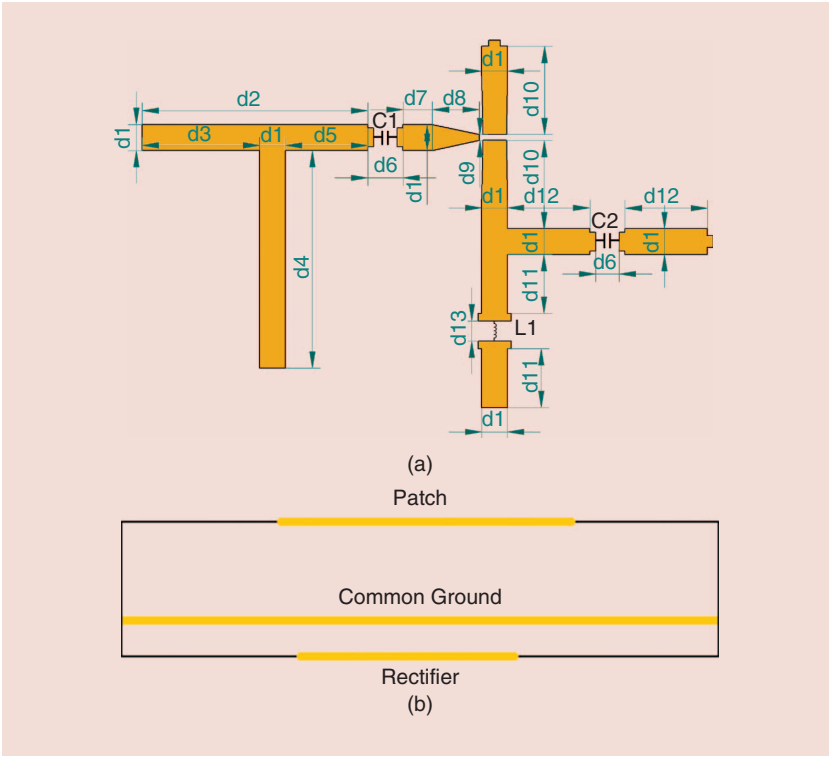

FIGURE 10. (a) The layout of the Wi-Fi rectifier and (b) a side view of the combined patch/rectifier configuration in a multilayer substrate.

TABLE 2. THE DIMENSIONS FOR THE PATCH RECTIFIER.

Parameter	Value	Parameter	Value
d1	2.2 mm	d9	0.5 mm
d2	19.2 mm	d10	7.5 mm
d3	10 mm	d11	5 mm
d4	18.5 mm	d12	7 mm
d5	7 mm	d13	1.7 mm
d6	3 mm	C1	100 nF
d7	2.5 mm	C2	100 nF
d8	4	L1	22 nH

$$\eta_{\text{diff}} = \frac{(2V_{\text{dc}})^2}{2P_{\text{RF}}R_{\text{Load}}} = 2\eta. \qquad (3)$$

Zero-bias Schottky diodes are used in the rectifier circuit because they have very low forward voltage drop [19]. However, the impedance of these diodes has a very large imaginary part for the power levels considered for harvesting. This complicates the process of matching the antennas to the rectifying circuits (especially for the wide-band matching needed for the LTSA), which is necessary to minimize power losses.

The overall structure contains 24 antenna ports (16 for Wi-Fi and eight for cellular) that are connected to their corresponding rectifiers, constituting a 12-differential pair system. This corresponds to eight differential voltage sources for the Wi-Fi band rectenna module and four differential voltage sources for the cellular rectenna module. In the following sections, the design procedure together with simulated and measured performance of the two subsystems is presented in detail. The antennas were designed using CST Microwave Studio and the rectifiers using Keysight's Advanced Design System.

The power combining from all rectennas is implemented with a dc series combiner, as depicted in Figure 6. The energy can be stored in a supercapacitor. Super- or ultracapacitors are preferred because they can charge and discharge a large number of times [20]. They also operate with almost no losses due to low inner resistance. Another advantage is their quick charge and discharge speed. Batteries have the ability to store a larger amount of energy than supercapacitors for the same volume. But a supercapacitor's storage capabilities are sufficient for this application, and with all of the other benefits for capacitors, they outweigh the advantages that batteries might have. Supercapacitors are also in general more environmentally friendly. Printed supercapacitors are also a feasible solution for future harvesting applications [21] together with printed rectennas.

DESIGN PROCEDURE OF THE RECTIFIERS

The construction of the rectifiers was made with an in-house etching process. It was observed that uncertainties in the construction procedure could have significant impact on the overall performance of the system. Therefore, a sensitivity analysis was performed to assess how different variations in the rectifier dimensions could affect the result. The rectifiers can be divided into two main parts: the RF part that corresponds to the matching network (to the left of the diode pair in the inset of Figure 7) and the dc part that corresponds to the circuitry after the diode component (to the right of the diode pair in the inset of Figure 7).

To ensure stability in the solution, the length of the stub in the matching network was varied ±0.5 mm in the simulations. The matching should not change drastically at the desired frequency. A maximum frequency shift of ~50 MHz was seen for the changes in stub length.

The impedance of the dc part should ideally remain stable with varying dimensions of the connecting microstrip lines. Its stability is important for the matching

network to maintain its function. However, higher-order harmonics can be generated by nonlinear components, such as the diodes that are used, and this may cause the impedance to be dependent on the dimensions of the dc transmission lines. A sensitivity analysis of the dc part was conducted, varying the lengths and widths of the lines to ensure that our impedance will remain stable. To illustrate this, a linear sweep, from 3 to 7 mm with a step size of 0.8 mm, of one microstrip length L at the dc part of the single-band rectifier is depicted in Figure 7. It is observed that the impedance changes rapidly at first but converges as the length increases. This process was performed on all of the microstrip components on the dc part.

WI-FI RECTENNA

Patch antennas were selected for harvesting the Wi-Fi band. They can achieve about 9-dB gain with above 90% efficiency [18] when they are constructed on a low-loss and low dielectric constant material. They are also robust and easy to manufacture. The main drawback with patch antennas is their relatively narrow bandwidth and beamwidth. Because Wi-Fi harvesting is mainly aimed at indoor applications, the harvester is going to be placed in a rich scattering and polarization environment. Taking into account all of these aspects as design constraints, a square dual-polarized X-slot loaded patch antenna is designed and placed in pairs on the four faces of the cuboid. In Figure 8, a pair is depicted with the corresponding dimensions listed in Table 1.

The X-slot loading of the patch enabled a miniaturization of the design, and it also decreased the levels of the cross-polar component, which improved the capturing of signals in a rich scattering environment. The X-slot loading reduced the size by approximately 5% and the cross-polar component by 3 dB. The patches are handmade using a Rohacell 71HF foam with $\varepsilon_r = 1.07$ and $\tan\delta = 0.0002$. The simulated and measured gain and reflection coefficient are depicted in Figure 9.

The reflection measurement was obtained using a portable Anritsu MS2016B vector network analyzer with the remaining ports terminated. The element patterns were measured with a near-field scanner from EMSCAN RFxpert.

The rectifier for the patch is matched from a 50-Ω antenna input to the impedance of the diode as determined by harmonic balance. The matching network consists of an open circuited stub in a half T-network configuration. The layout is depicted in Figure 10(a), and the dimensions are listed in Table 2. The Wi-Fi rectifier is constructed in a polytetrafluoroethylene (PTFE) substrate with 0.8-mm thickness and $\varepsilon_r = 2.4$.

The output efficiency depends on the load that is used. This is illustrated, together with the reflection coefficient and the output voltage for –15-dBm

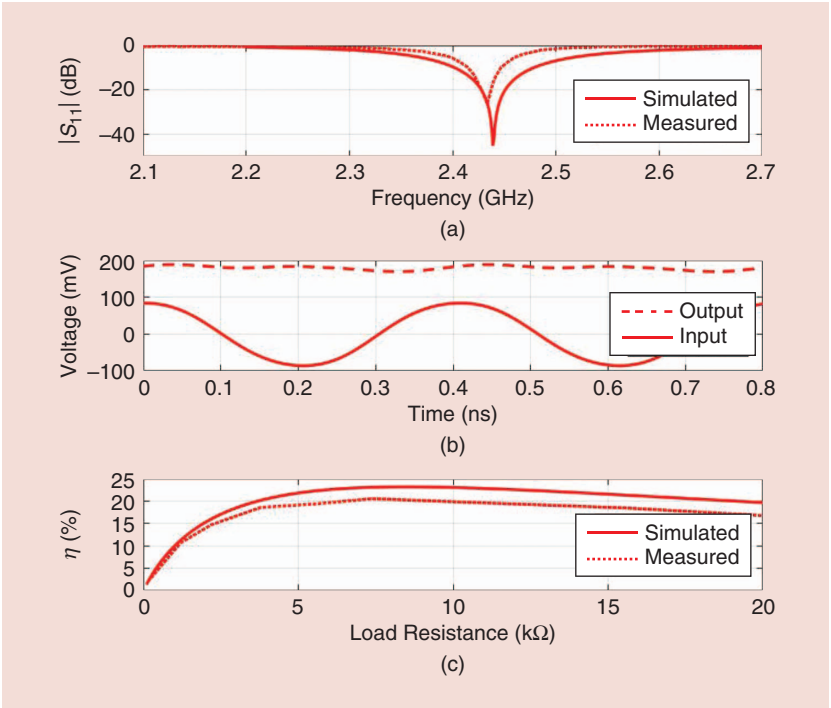

FIGURE 11. The Wi-Fi rectifier performance: (a) simulated and measured $|S_{11}|$, (b) voltage input and output with –15-dBm input power, and (c) efficiency versus load resistance for –15-dBm input power, measured and simulated, at 2.45 GHz.

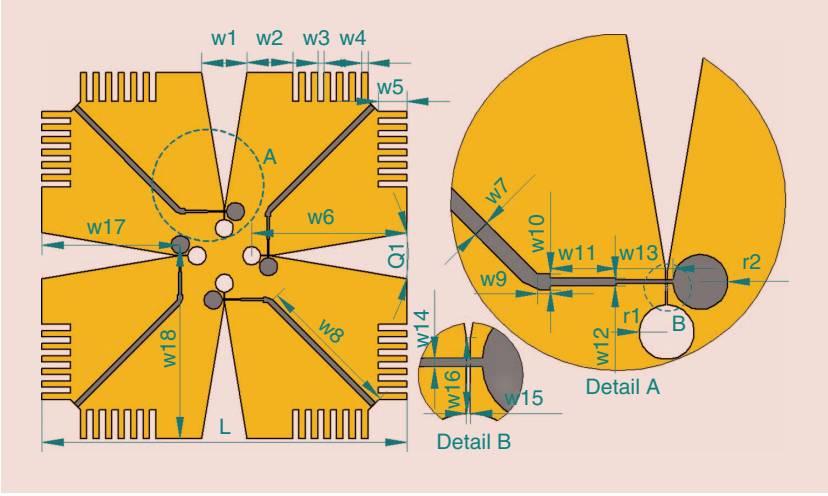

FIGURE 12. The layout of a set of four LTSAs. Note that the feeds (gray) and the ground plane (yellow) are separated by a dielectric substrate.

TABLE 3. THE DIMENSIONS FOR THE LTSA.

Parameter	Value	Parameter	Value
w1	31 mm	w12	2.9 mm
w2	40.25 mm	w13	26.9 mm
w3	5.83 mm	w14	1.5 mm
w4	5.67 mm	w15	0.65 mm
w5	25.5 mm	w16	12 mm
w6	126 mm	w17	105.7 mm
w7	5.6 mm	w18	179.53 mm
w8	106 mm	L	320 mm
w9	5.5 mm	r1	14 mm
w10	5.6 mm	r2	13 mm
w11	26.2 mm	a1	17.62°

input power, in Figure 11. The optimal load for the Wi-Fi rectenna is determined as 8 kΩ.

To have both the antenna and the rectifier ports accessible for measurements, they have been constructed separately and connected with a cable. Ideally, this should be configured with common ground configuration, as depicted in Figure 10(b). In this configuration, additional effort to match the exact output impedance of the antenna to the rectifier and connecting them with a through via would be necessary.

CELLULAR RECTENNA

To cover the cellular band, we use a variation of the LTSA on the two remaining faces. The LTSA radiates at the endfire direction and has a wider beamwidth as compared to patch antennas. Thus, only one antenna per sector was used in this case. Each LTSA is fed with a 50-Ω microstrip line that is transformed to 100 Ω with a stepped impedance transformer and is terminated in a wideband open-circuited circular stub. The microstrip line feeds the slot through aperture coupling. The slot opens to a linear tapered flare slot from one side and is terminated in a circular short circuited slot stub on the other side. The proposed LTSA configuration is fairly easy to construct, and it is also very compact, with four antennas confined within 320×320 mm^2.

Corrugations have been introduced along the edges of the LTSA, as illustrated in Figure 12 with dimensions listed in Table 3. These corrugations act as a soft surface [22] to reduce the propagation along the edges. In Figure 13, the $|S_{11}|$ of the LTSA is depicted, where we compare the simulated version with and without corrugations and the measured data of a single LTSA in the system with the rest of the ports terminated. The measured antenna has a bandwidth of approximately 35% with $|S_{11}| = -10$ dB and a central frequency of 2.05 GHz. The difference of the radiation patterns with and without corrugations is depicted in Figure 14. The LTSA antenna is constructed in a substrate based on polypropylene with 1.5-mm thickness and $\varepsilon_r = 3$. The corrugations improve the gain by ~3 dB

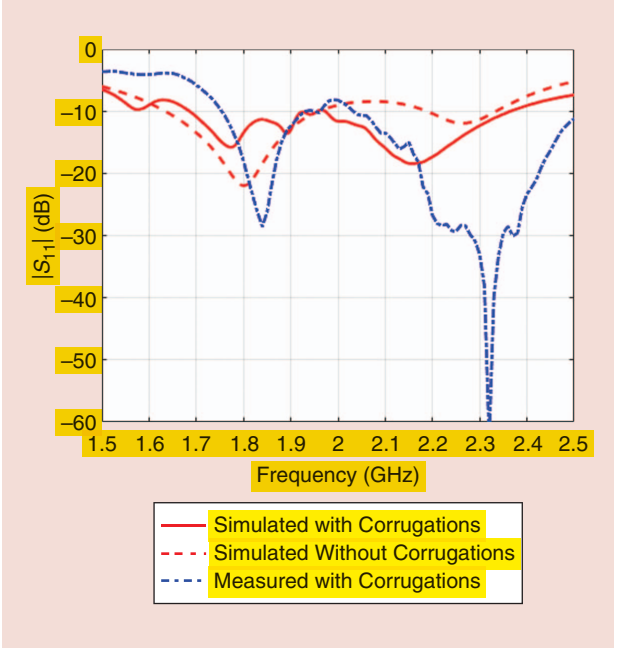

FIGURE 13. The simulated and measured $|S_{11}|$ for the LTSA, with and without corrugations.

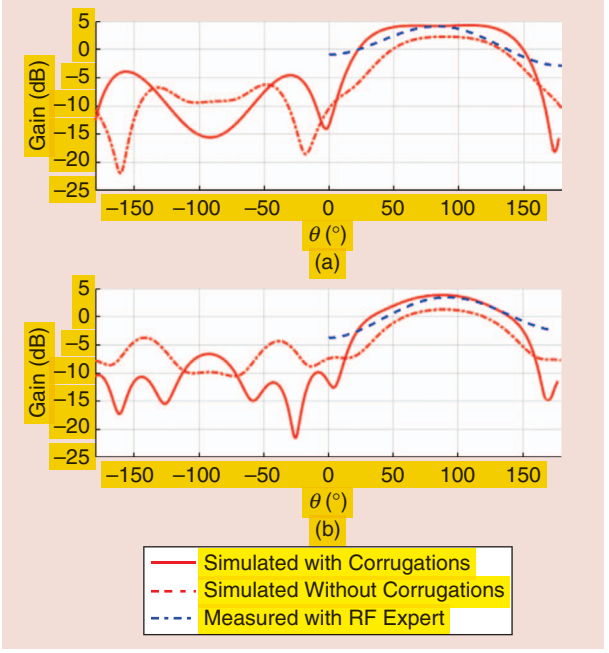

FIGURE 14. The simulated and measured far field (E-plane) for the LTSA: (a) 2.15 GHz and (b) 1.8 GHz.

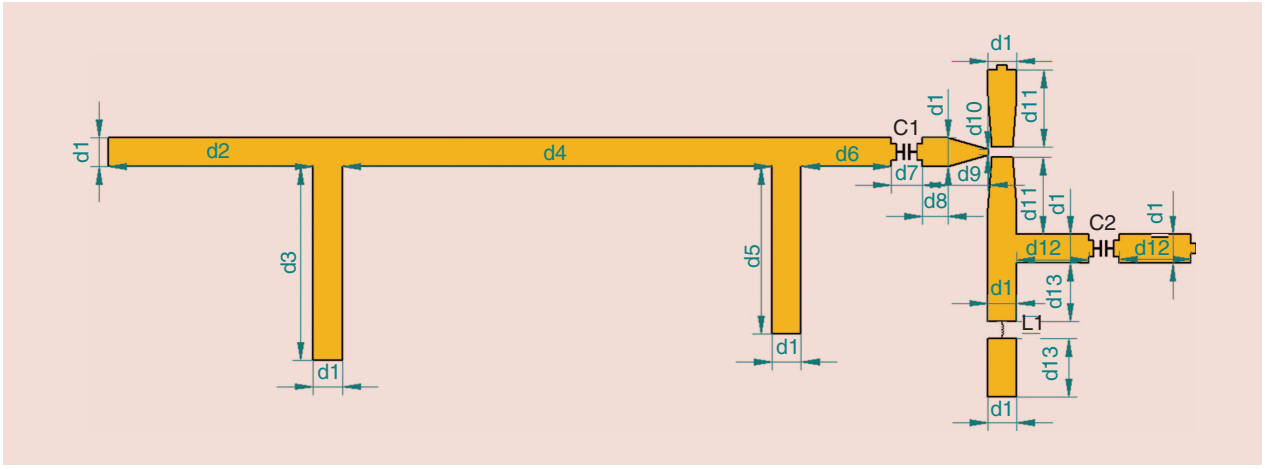

FIGURE 15. The layout of the LTSA rectifier.

and also reduce the sidelobes by ~5 dB on average.

For the cellular rectification, we found, during our measurement campaign, two different narrow cellular bands: 3G, 2.1 GHz, and GSM, 1.8 GHz. We decided to accommodate both of these two bands and design a dual-band rectifier. The design of the final layout of the rectifier is illustrated in Figure 15. We used two half T-networks to match the two bands, and the dimensions of the rectifier are listed in Table 4. The cellular rectifier is constructed on an FR4 substrate with a thickness of 1.5 mm. The input reflection coefficient, the voltage output, and the efficiency for the cellular rectifier are depicted in Figure 16. The optimal load for the cellular rectenna is 4 kΩ.

Ideally, all of the circuitry should be placed on the same printed circuit board (PCB) as the antenna to minimize connection losses. We have already taken that into account and allocated enough space to place them directly after the antenna ports. Here, we use an RF-coaxial connector at the input of the antennas and cable connections to the input of the rectifiers.

SYSTEM PERFORMANCE EFFICIENCY CHARACTERIZATIONS

The complete system and the two submodules are depicted in Figure 17. The patch antennas of the system are not affected by the cuboid configuration, whereas the LTSA is affected mostly at 1.8 GHz, and parasitic lobes appear in the radiation pattern. These parasitic lobes will not impact the performance of the system and only alter the peak gain of the antenna. The embedded total efficiency for the LTSA and the patch are $\eta_{LTSA} = 80\%$ and $\eta_{patch} = 90\%$, respectively. The installed radiation patterns are depicted in Figure 18. In Figure 19, the developed PCBs for the rectifiers for cellular and Wi-Fi bands are depicted.

The efficiency of the harvesting system depends mostly on the rectifier efficiency, as $\eta_{sys} = \eta_{ant} \times \eta_{rect}$. The proposed rectifier efficiencies are presented in Figures 11 and 16, with the peak efficiency for all bands summarized in Table 5. A comparison with some state-of-the-art rectifiers operating at similar frequencies and input powers is also included in the table. As can be seen, the obtained rectifier efficiency is comparable with state-of-the-art designs [4], [8], [23], [24], and [26]. For the cellular band, our design suffers losses due to the use of FR4 instead of PTFE.

To characterize our design in a real environment, the modular components that were designed and constructed in the previous sections are now combined to a full system. As stated, we have considered five different location scenarios for the system: indoors, semi-indoors, outdoors, semi-outdoors, and basements or underground laboratories. We have devised the following procedure for each subsystem to simplify the measurement evaluation for the input power. For the Wi-Fi rectenna module, we measured the power delivered in the antennas using the spectrum analyzer and a four-port power divider available in our laboratory. We combine four ports covering half-azimuthal plane for a single polarization. We perform this measurement four times to cover the full space and both polarizations. The antenna ports that are not used in each case are matched with 50-Ω resistive terminations. We combine the input power levels from all four measurements

TABLE 4. THE DIMENSIONS FOR THE CELLULAR RECTIFIER.

Parameter	Value	Parameter	Value
d1	2 mm	d9	4 mm
d2	10 mm	d10	0.5 mm
d3	26.5 mm	d11	7.5 mm
d4	38 mm	d12	9 mm
d5	16.8 mm	d13	7.5 mm
d6	5.5 mm	C1	100 nF
d7	3 mm	C2	100 nF
d8	2.5 mm	L1	22 nH

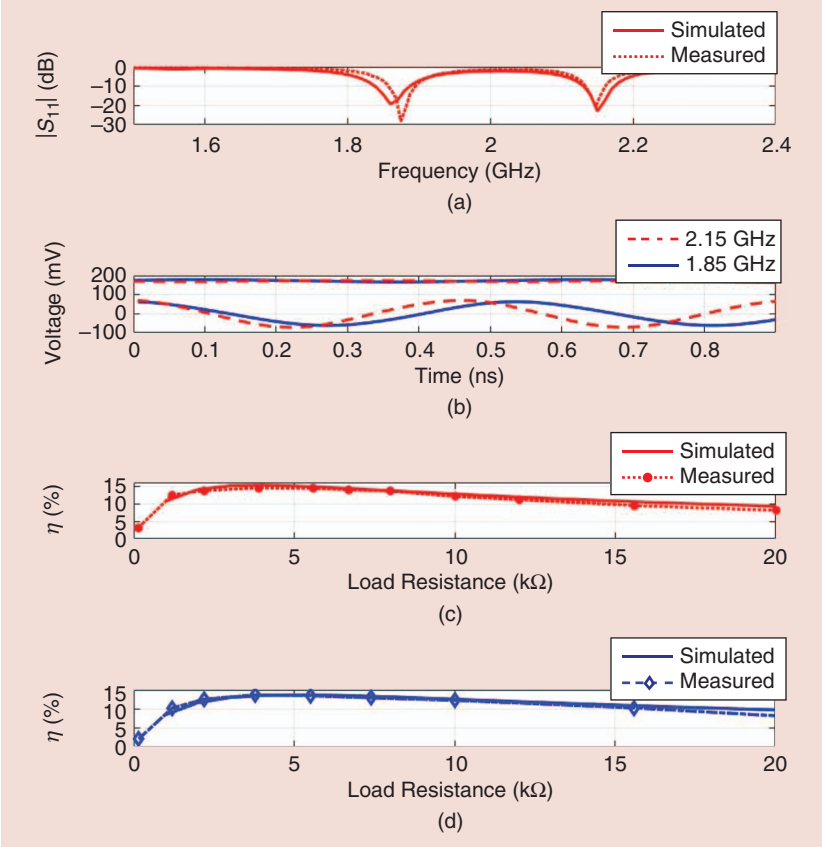

FIGURE 16. The cellular rectifier performance: (a) simulated and measured $|S_{11}|$ and (b) voltage when input power is –15 dBm. Efficiency versus load resistance for –15-dBm input power, measured and simulated at (c) 1.85 GHz and (d) 2.15 GHz.

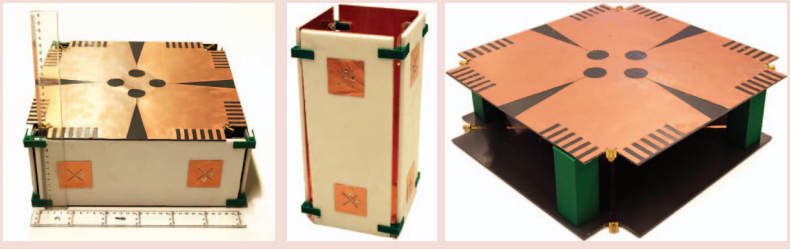

FIGURE 17. The realized RF harvesting system and the modules for cellular and Wi-Fi harvesting. The overall dimensions of the system are $320 \times 320 \times 150$ mm^3. The (a) full system, (b) Wi-Fi module, and (c) cellular module.

TABLE 5. THE PEAK RECTIFIER EFFICIENCY OBTAINED AT –15-dBm INPUT POWER.

	1.85 GHz (%)	2.15 GHz (%)	2.45 GHz (%)
Our design	13	15	20
Reference designs	15 (–20 dBm) [23]	23 [24]	7 [25]
	7 (–10 dBm) [8]	5 (–10 dBm) [8]	15 (–20 dBm) [26]
			28 (–20 dBm) [4]

Values in parentheses are alternative input powers.

assuming that this is the available input power for our antenna system. Here, it is worth noting that coupling between RF signals in the terminated ports is not included, which makes this measurement an underestimation.

The available input power for each subsystem at each scenario is listed in Table 6. In the last column, the combined output power is stated. From the table, it is also clearly illustrated which systems have been used at each scenario. For simplicity, during the measurements for the different scenarios the system was kept in the same configuration as in Figure 17(a), obtaining only the relevant outputs at each scenario.

For the cellular rectenna, we follow a similar procedure and measure the full azimuthal plane from all four LTSA antennas with the difference that only a single measurement is required to achieve a full azimuthal coverage. Because we used two identical LTSA configurations, we double the available input power. Both measurements with the four-port divider yield an underestimation for the system performance, as this excites an inherent circular array mode. This illustrates the advantages of our approach to rectify each antenna separately and combine the dc outputs.

CONCLUSIONS

A modular RF energy harvester has been designed, constructed, and measured. The main intended application of the proposed system is smart building sensing. However, the system is not only limited to this application, and it could be easily extended to sensor networks in, e.g., smart factories and vehicles.

The antennas of the system, LTSA and patches, cover from 1.7 to 2.5 GHz and 2.4 to 2.5 GHz, respectively. The corresponding rectifiers can extract usable dc voltages at the 1.85-GHz (GSM) and 2.15-GHz (3G) frequencies and full Wi-Fi, all available at the KTH campus. A novel MISO approach was used for the full-wave rectification to extract differential dc voltages from low RF levels. The total size of the full system is $320 \times 320 \times 150$ mm^3. The system is modular, so it becomes smaller if only one of the bands is available.

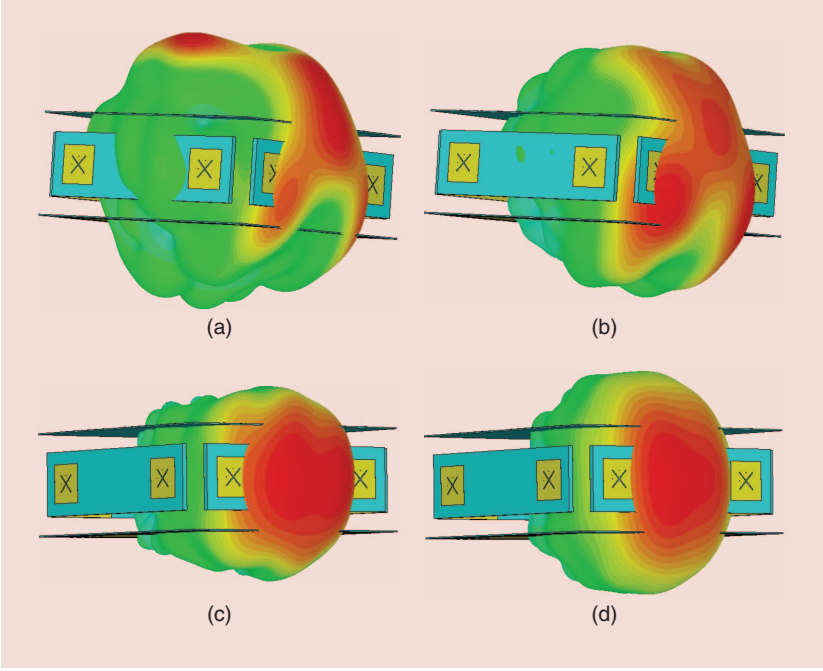

FIGURE 18. The simulated 3-D radiation patterns. From LTSA on the top face at (a) 1.8 GHz and (b) 2.1 GHz and from the patch antenna at 2.45 GHz, (c) horizontal polarization, and (d) vertical polarization.

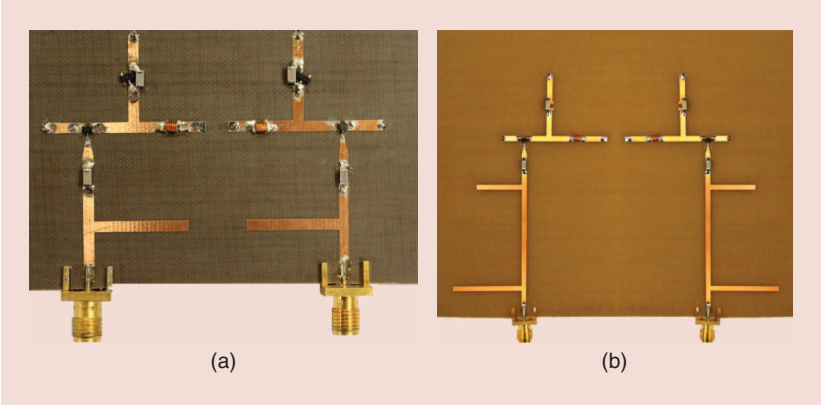

FIGURE 19. The realized rectifiers for the RF harvesting system for Wi-Fi and cellular bands. The overall dimensions of the system are $320 \times 320 \times 150$ mm^3. (a) Wi-Fi rectifier and (b) cellular rectifier.

TABLE 6. THE SYSTEM MEASUREMENTS FOR AVAILABLE RF POWER AND THE COMBINED OUTPUT POWER.

	Wi-Fi (dBm)	Cellular (dBm)	Combined Output Power (μW)
Indoors	–22	–27	5.2
Semi-indoors	–30	–25	2.1
Outdoors	—	–20	1.7
Semi-outdoors	–40	–23	4.2
Underground	–20	—	4.6

ACKNOWLEDGMENTS

We thank everyone in the Electromagnetic Engineering Department at KTH Royal Institute of Technology in Stockholm, Sweden, who provided the lab facilities for construction and measurement and especially Janne Nilsson for his great and necessary contribution to the rectifier circuit. Also, we thank Jesper Freiberg for his help during the construction process. Finally, we would like to thank all of the people involved in the IEEE Antennas and Propagation Student Design Contest for their efforts and excellent organization.

AUTHOR INFORMATION

O. Björkqvist (oskarbjo@kth.se) is a student at the School of Electrical Engineering, KTH Royal Institute of Technology, Stockholm, Sweden.

O. Dahlberg (oskdah@kth.se) is a student at the School of Electrical Engineering, KTH Royal Institute of Technology, Stockholm, Sweden.

G. Silver (gsilver@kth.se) is a student at the School of Electrical Engineering, KTH Royal Institute of Technology, Stockholm, Sweden.

C.I. Kolitsidas (chko@kth.se) is a Ph.D. student at the School of Electrical Engineering, KTH Royal Institute of Technology, Stockholm, Sweden. He is the corresponding author of this article.

O. Quevedo-Teruel (oscarqt@kth.se) is an associate professor with the School of Electrical Engineering, KTH Royal Institute of Technology, Stockholm, Sweden.

B.L.G. Jonsson (ljonsson@kth.se) is a professor with the School of Electrical Engineering, KTH Royal Institute of Technology, Stockholm, Sweden.

REFERENCES

[1] C. R. Valenta and G. D. Durgin, "Harvesting wireless power: Survey of energy-harvester conversion efficiency in far-field, wireless power transfer systems," *IEEE Microw. Mag.*, vol. 15, no. 4, pp. 108–120, 2014.

[2] D. Masotti, A. Costanzo, M. Del Prete, and V. Rizzoli, "Genetic-based design of a tetra-band high-efficiency radio-frequency energy harvesting system," *IET Microw. Antennas Propag.*, vol. 7, no. 15, pp. 1254–1263, 2013.

[3] M. Arrawatia, M. S. Baghini, and G. Kumar, "Differential microstrip antenna for RF energy harvesting," *IEEE Trans. Antennas Propag.*, vol. 63, no. 4, pp. 1581–1588, 2015.

[4] U. Olgun, C. C. Chen, and J. L. Volakis, "Investigation of rectenna array configurations for

enhanced RF power harvesting," *IEEE Antennas Wireless Propag. Lett.*, vol. 10, pp. 262–265, 2011.
[5] K. Nishida, Y. Taniguchi, K. Kawakami, Y. Homma, H. Mizutani, M. Miyazaki, H. Ikematsu, and N. Shinohara, "5.8 GHz high sensitivity rectenna array," in *Proc. 2011 IEEE MTT-S Int. Microwave Workshop Series Innovative Wireless Power Transmission: Technologies, Systems, and Applications (IMWS)*, pp. 19–22.
[6] M. Arrawatia, M. S. Baghini, and G. Kumar, "Broadband bent triangular omnidirectional antenna for RF energy harvesting," *IEEE Antennas Wireless Propag. Lett.*, vol. 15, pp. 36–39, 2016.
[7] Y. J. Ren, M. F. Farooqui, and K. Chang, "A compact dual-frequency rectifying antenna with high-orders harmonic-rejection," *IEEE Trans. Antennas Propag.*, vol. 55, no. 7, pp. 2110–2113, 2007.
[8] M. Arrawatia, M. S. Baghini, and G. Kumar, "Broadband RF energy harvesting system covering CDMA, GSM900, GSM1800, 3G bands with inherent impedance matching," in *Proc. IEEE MTT-S Int. Microwave Symp. (IMS)*, 2016, pp. 1–3.
[9] H. J. Visser and R. J. M. Vullers, "RF energy harvesting and transport for wireless sensor network applications: Principles and requirements," *Proc. IEEE*, vol. 101, no. 6, pp. 1410–1423, 2013.
[10] S. S. B. Hong, R. B. Ibrahim, M. H. M. Khir, M. A. B. Zakariya, and H. Daud, "Wi-Fi energy harvester for low power RFID application," *Prog. Electromagnetics Res. C*, vol. 40, pp. 69–81, 2013.
[11] M. Piñuela, P. D. Mitcheson, and S. Lucyszyn, "Ambient RF energy harvesting in urban and semi-urban environments," *IEEE Trans. Microw. Theory Techn.*, vol. 61, no. 7, pp. 2715–2726, 2013.
[12] C. Meneses Ghiglino, "Ultra-wideband (UWB) rectenna design for electromagnetic energy harvesting," M.S. thesis, Barcelona School of Telecommunications Engineering, Spain, 2010.
[13] F. Zhang, F. S. Zhang, G. Zhao, C. Lin, and Y. C. Jiao, "A loaded wideband linearly tapered slot antenna with broad beamwidth," *IEEE Antennas Wireless Propag. Lett.*, vol. 10, pp. 79–82, 2011.
[14] J. Wu, Z. Zhao, J. Liu, Z.-P. Nie, and Q. H. Liu, "A compact linear tapered slot antenna with integrated balun for UWB applications," *Prog. Electromagnetics Res. C*, vol. 29, pp. 163–176, 2012.
[15] C. Song, Y. Huang, J. Zhou, J. Zhang, S. Yuan, and P. Carter, "A high-efficiency broadband rectenna for ambient wireless energy harvesting," *IEEE Trans. Antennas Propag.*, vol. 63, no. 8, pp. 3486–3495, 2015.
[16] V. Marian, B. Allard, C. Vollaire, and J. Verdier, "Strategy for microwave energy harvesting from ambient field or a feeding source," *IEEE Trans. Power Electron.*, vol. 27, no. 11, pp. 4481–4491, 2012.
[17] Y. Yang, Y. Wang, and A. E. Fathy, "Design of compact Vivaldi antenna arrays for UWB see through wall applications," *Prog. Electromagnetics Res.*, vol. 82, pp. 401–418, 2008.
[18] C. A. Balanis, *Antenna Theory Analysis and Design*, 3rd ed. Hoboken, NJ: Wiley, 2005.
[19] Avago. (2016). HSMS-2852 data sheet. [Online]. Available: http://docs.avagotech.com/docs/AV02-1377EN
[20] J. R. Miller and P. Simon, "Electrochemical capacitors for energy management," *Science*, vol. 321, no. 5889, pp. 651–652, 2008.
[21] S. Lehtimäki, *Printed Supercapacitors for Energy Harvesting Applications*. Tampere, Finland: Tampere Univ. of Technology, 2017.
[22] Z. Ying, P. S. Kildal, and A. A. Kishk, "Study of different realizations and calculation models for soft surfaces by using a vertical monopole on a soft disk as a test bed," *IEEE Trans. Antennas Propag.*, vol. 44, no. 11, pp. 1474–1481, 1996.
[23] A. Collado and A. Georgiadis, "Conformal hybrid solar and electromagnetic (EM) energy harvesting rectenna," *IEEE Trans. Circuits Syst. I, Reg. Papers*, vol. 60, no. 8, pp. 2225–2234, 2013.
[24] A. Khemar, A. Kacha, H. Takhedmit, and G. Abib, "Design and experiments of a 3G-band rectenna for radio frequency energy harvesting," *Rev. Roum. Sci. Tech. Ser. Electrotech. Energ.*, vol. 62, no. 1, pp. 82–86, 2017.
[25] D. Wang and R. Negra, "Design of a rectifier for 2.45 GHz wireless power transmission," in *Proc. 2012 8th Conf. Ph. D. Research in Microelectronics and Electronics (PRIME)*, pp. 1–4.
[26] A. Georgiadis, G. V. Andia, and A. Collado, "Rectenna design and optimization using reciprocity theory and harmonic balance analysis for electromagnetic (EM) energy harvesting," *IEEE Antennas Wireless Propag. Lett.*, vol. 9, pp. 444–446, 2010.

CHAPTER NEWS

(continued from page 12)

and Techniques, Electron Devices, Aerospace and Electronic Systems, and Communications Joint Societies Chapter
- approval date: 13 April 2018
- geocode: CH02150

7) IEEE Beijing Section AP-S Shenzhen Chapter
- approval date: 6 May 2018
- geocode: CH10854

8) IEEE Madras Section St. Joseph's Institute of Technology AP-S SB Chapter
- approval date: 20 May 2018
- geocode: SBC16181F

9) IEEE Kharagpur Section-Indian Institute of Engineering Science and Technology, Shibpur AP-S SB Chapter
- approval date: 25 May 2018
- geocode: SBC20125C

10) IEEE Delhi Section-Indian Institute of Technology Jodhpur AP-S SB Chapter
- approval date: 28 May 2018
- geocode: SBC15133

11) IEEE Kolkata Section-National Institute of Technology-Silchar AP-S SB Chapter in the Kolkata Section
- approval date: 7 June 2018
- geocode: SBC03701B

12) IEEE Romania Section AP-S and Council on RFID Joint Chapter
- approval date: 22 June 2018
- geocode: CH08832

13) IEEE Delhi Section Manipal University AP-S SB Chapter
- approval date: 9 July 2018
- geocode: SBC13611C

14) IEEE Madras Section K. Ramakrishnan College of Engineering AP-S SB Chapter
- approval date: 23 July 2018
- geocode: SBC64616B.